Environment International 163 (2022) 107200

Contents lists available at ScienceDirect

Environment International

journal homepage: www.elsevier.com/locate/envint

Full length article

Human airway organoids and microplastic fibers: A new exposure model for emerging contaminants

Anna Sophie Winkler [a], Alessandro Cherubini [c,1], Francesco Rusconi [c,1], Nadia Santo [b,1], Laura Madaschi [b,1], Clelia Pistoni [c], Giorgia Moschetti [d], Maria Lucia Sarnicola [d], Mariacristina Crosti [d], Lorenzo Rosso [e], Paolo Tremolada [a], Lorenza Lazzari [c,*], Renato Bacchetta [a,*]

[a] Department of Environmental Science and Policy, University of Milan, Via Celoria 26, 20133 Milan, Italy
[b] Unitech NOLIMITS, Imaging Facility, University of Milan, Via Golgi 19, 20133 Milan, Italy
[c] Laboratory of Regenerative Medicine - Cell Factory, Department of Transfusion Medicine and Hematology, Fondazione IRCCS Ca' Granda Ospedale Maggiore Policlinico, Via Francesco Sforza 35, 20122 Milan, Italy
[d] Istituto Nazionale Genetica Molecolare INGM 'Romeo ed Enrica Invernizzi', Via Francesco Sforza 35, 20122 Milan, Italy
[e] Department of Pathophysiology and Transplantation, University of Milan and Thoracic Surgery and Transplantation Unit, Fondazione IRCCS Ca Granda Ospedale Maggiore Policlinico, Via Francesco Sforza 35, 20122 Milan, Italy

ARTICLE INFO

Handling Editor: Adrian Covaci

Keywords:
Airway organoids
Airborne microplastic
Polyester fibers
Dryer machine

ABSTRACT

Three-dimensional (3D) structured organoids are the most advanced *in vitro* models for studying human health effects, but their application to evaluate the biological effects associated with microplastic exposure was neglected until now. Fibers from synthetic clothes and fabrics are a major source of airborne microplastics, and their release from dryer machines is poorly understood. We quantified and characterized the microplastic fibers (MPFs) released in the exhaust filter of a household dryer and tested their effects on airway organoids (1, 10, and 50 μg mL^{-1}) by optical microscopy, scanning electron microscopy (SEM), confocal microscopy and quantitative reverse transcription–polymerase chain reaction (qRT-PCR). While the presence of MPFs did not inhibit organoid growth, we observed a significant reduction of SCGB1A1 gene expression related to club cell functionality and a polarized cell growth along the fibers. The MPFs did not cause relevant inflammation or oxidative stress but were coated with a cellular layer, resulting in the inclusion of fibers in the organoid. This effect could have long-term implications regarding lung epithelial cells undergoing repair. This exposure study using human airway organoids proved suitability of the model for studying the effects of airborne microplastic contamination on humans and could form the basis for further research regarding the toxicological assessment of emerging contaminants such as micro- or nanoplastics.

1. Introduction

Atmospheric contamination through airborne particles and fibers is a long-existing and growing research topic of environmental pollution. Several epidemiological studies have already linked air pollution through ambient atmospheric particulate matter to many adverse human health effects, including respiratory illness, cardiovascular disease, and carcinogenic effects (Churg and Bauer, 2000; Loomis et al., 2013; Valavanidis et al., 2008). In addition to the well-known air pollutants such as combustion particles from fuel-burning emissions and other particulate organic matter and aerosols (Nel, 2005), microplastics (MPs) are now considered as emerging components of air pollution (Zhang et al., 2020).

The human health effects of MPs and nanoplastics (NPs) are usually

Abbreviations: ATR-FTIR, attenuated total reflection Fourier transform infrared spectroscopy; hAO, human airway organoid; hPO, human pancreas organoid; MP, microplastic; MPF, microplastic fiber; NP, nanoplastic; qRT-PCR, quantitative reverse transcription–polymerase chain reaction; SEM-EDS, scanning electron microscope - energy dispersive x-ray spectroscopy.

* Corresponding authors.
E-mail addresses: lorenza.lazzari@policlinico.mi.it (L. Lazzari), renato.bacchetta@unimi.it (R. Bacchetta).
[1] These authors contributed equally to this work.

https://doi.org/10.1016/j.envint.2022.107200
Received 16 October 2021; Received in revised form 1 March 2022; Accepted 21 March 2022
Available online 26 March 2022

deduced from *in vivo* exposure tests in animal models, i.e., mammalian or nonmammalian models such as mice, rats, *Xenopus laevis* (De Felice et al., 2018), and zebrafish (Bhagat et al., 2020), and from *in vitro* models such as human cell cultures. After exposure, i.e., inhalation or ingestion, MPs/NPs may pass through biological barriers, leading to translocation in the body tissue. The cell uptake, however, is size-dependent; it has been proven that cell internalization increases with decreasing particle size (Liu et al., 2021) with an assumed upper particle size limit for intracellular uptake of 10 μm (for polyethylene), (Bruinink et al. (2015)). Indeed, the transfer of MPs/NPs into human cells has been demonstrated using a variety of human cell lines, including epidermal cells (Triebskorn et al., 2019), lung epithelial cells (Lim et al., 2019; Schirinzi et al., 2017; Xu et al., 2019), endothelial cells (Barshtein et al., 2016), and intestinal cells (Cortés et al., 2020; Domenech et al., 2020). Human two-dimensional (2D) cell cultures are common *in vitro* models used to evaluate the biological effects associated with MP/NP exposure; however, these systems have some limitations such as an inaccurate representation of the *in vivo* tissue (Costa et al., 2016). Very recently, organoids, which are three-dimensional (3D) cellular structures generated from induced pluripotent stem cells, embryonic stem cells, or adult tissue-resident stem cells (Shamir and Ewald, 2014) have been shown to be a powerful tool to overcome the limits of 2D culture. Indeed, organoids, such as kidney (Takasato et al., 2016), brain (Lancaster et al., 2013), intestine (Sato et al., 2011), liver (Huch et al., 2015), pancreas (Dossena et al., 2020) and lung (Sachs et al., 2019) organoids, have recently emerged as attractive model systems that contain key aspects of *in vivo* tissue and organ complexity while being more experimentally manageable than model organisms. Moreover, these 3D structures have been recently applied in nanosafety research (Kämpfer et al., 2020) and modeling diseases such as cancer (Tuveson and Clevers, 2019).

MPs are ubiquitous in the environment (Prata et al., 2020a; 2020b). In the atmosphere, the largest proportion of the MPs consists of microplastic fibers (MPFs) derived from various sources, including synthetic clothes, textiles, and upholstery (Henry et al., 2019). Especially indoor, airborne MPF pollution arises from the wear and tear of clothing, carpets, and furniture (e.g., polyester, nylon, acrylic, and polyamide) (Akanyange et al., 2021), with synthetic clothing mostly made of polyethylene terephthalate (namely, polyester) as the largest source of airborne MPs (Dris et al., 2016). Furthermore, Dris et al. (2017) and Liu et al. (2019) have investigated and compared MPFs in indoor and outdoor air. They found that indoor air contains considerably higher amounts of natural and synthetic fibers than outdoor air and dust, with an indoor fiber concentration ranging from 1.0 to 60.0 fibers m^{-3} (Dris et al., 2017). Also Gaston et al. (2020) found that the interior air space (9.8 ± 7.3 fibers per m^{-3}) was significantly more enriched with MPFs relative to the outdoor space outdoors. As Rist et al. (2018) already pointed out, airborne MPF from synthetic clothes represent an important contribution to the total MP exposure pathways, especially considering that people spend most of their lifetime indoors (Akanyange et al., 2021). Recent studies also have demonstrated that a major pathway for MPFs is the atmosphere, through which they can reach very remote areas such as glaciers (Ambrosini et al., 2019), the Arctic region (Bergmann et al., 2017; Lusher et al., 2015), and Antarctica (Reed et al., 2018; Waller et al., 2017).

MPFs can be released into the wastewater through the washing of synthetic textiles and clothes, as demonstrated previously in several studies (Browne et al., 2011; De Falco et al., 2019). In addition to the washing process, the drying of synthetic textiles with a household clothes dryer further emits MPFs into the atmosphere via the exhaust air. However, the air contamination caused by the drying of synthetic clothes and fabrics is still poorly understood. Recently, O'Brien et al. (2020) have reported and quantified for the first time the amount of MPFs released from a clothes dryer into the ambient air. The issue was further addressed by Kapp and Miller (2020) who studied the spatial distribution of MPFs emitted from the vent of a clothes dryer directly into the environment.

Human inhalation of atmospheric MPFs has been demonstrated *in vivo* (human lung biopsies) by Pauly et al. (1998) and Pimentel et al. (1975). The deposition of MPs, however, depends on the properties and lung anatomy (Churg and Bauer, 2000; Lippmann et al., 1980). Currently, it is well known that humans in certain exposure scenarios, such as industrial workers, are particularly susceptible to pulmonary diseases caused by airborne synthetic fibers (Goldberg and Thériault, 1994; Mastrangelo et al., 2002). In the attempt to estimate the human inhalation of indoor airborne MPs, Vianello et al. (2019) set up a mannequin simulating the human metabolic rate and breathing (male person with light activity). The simulated human exposure revealed an average inhaled concentration of 9.3 ± 5.8 MPs m^{-3} (or 272 MPs per day), corresponding to the value of indoor airborne fibers reported by Dris et al. (2017) (median value of 5.4 fibers m^{-3}) and Gaston et al. (2020) (mean value of 9.8 ± 7.3 fibers m^{-3}) – disregarding the problem of comparing the results of studies using different analytical techniques.

The available data or information providing evidence of the negative human health effects of inhaled MPFs are still rare and insufficient (Prata, 2018). To date, the human exposure risk still remains unclear, and the consequences of MPF exposure are not yet well understood (Prata et al., 2020a; 2020b). Accordingly, there is an increasing demand for interdisciplinary research between environmental and human health sciences (Dris et al., 2017). In this study, we propose the application of the innovative human organoid model for human exposure tests for MPs/NPs and other particulate contaminants. Considering the described exposure risk for humans to airborne MPs, the use of the human lung airway as an organoid model in this study is an innovative experimental approach.

Importantly, exposure tests should apply environmentally relevant MP properties (Prata et al., 2020a; 2020b), such as fibrous or aged MPs. Therefore, to test the effects of airborne MPFs on human airway organoids (hAOs), polyester fibers emitted from the drying process of synthetic clothes and fabrics were collected and used as a test contaminant. The specific aims of this paper were as follows: i) to characterize the release of MPFs in the exhaust filter of a household dryer machine; ii) to analyze the effect of these environmentally relevant MPFs on hAOs as a possible target of airborne contamination from synthetic clothes; iii) to characterize the established hAOs; and iv) to evaluate the use of human organoid models to assess the effects of pollutants to humans.

2. Material and methods

2.1. hAO isolation and culture

The herein applied hAOs were generated from tissue-resident adult stem cells. Healthy human lung tissues (airway space) were obtained from the Thoracic Surgery and Lung Transplant Unit, IRCCS Ca' Granda Ospedale Maggiore Policlinico, Milan, Italy. The use of human specimens was approved by the Institutional Review Board (CE 0001977). Young patients underwent minimal invasive wedge lung resection for spontaneous pneumothorax.

For the processing of solid lung tissue, the biopsies (0.5–1 cm^3) were minced in small pieces and rinsed with wash medium (Dulbecco's modified Eagle medium, DMEM) supplemented with 1% fetal bovine serum, 1% penicillin/streptomycin and 1 × Glutamax (see Table S1 for the source and ID numbers of all reagents used). Fragments were digested in wash medium containing 0.125 mg mL^{-1} collagenase I, 0.125 mg mL^{-1} dispase II, and 0.1 mg mL^{-1} DNase I for 90 min at 37 °C. The digestion was stopped by adding cold wash medium, and the suspension was filtered through a 70-μm cell strainer and then spun for 5 min at 400*g*. In case of visible red pellets, erythrocytes were lysed in 5 mL of red blood cell lysis buffer for 15 min at room temperature before the addition of wash medium and centrifugation at 400*g*. The cell pellet was mixed with Matrigel, and 40 μL of Matrigel-cell suspension was allowed to solidify on prewarmed nontissue culture 24-well plates for 20–30 min. After complete Matrigel solidification, culture medium

containing AdDMEM/F12 supplemented with 10 mM Hepes, 1 × penicillin/streptomycin, 1 × Glutamax, 1% B27, 1.25 mM N-acetylcysteine, 25 ng mL^{-1} FGF7, 500 ng mL^{-1} RSPO1, 100 ng mL^{-1} FGF10, 100 ng mL^{-1} Noggin, 5 mM nicotinamide, 500 nM A83.01, and 500 nM SB202190 was added. For establishment of the organoids, the culture medium was supplemented with 10 μM Rock inhibitor Y27632 during the first three days. The culture medium was changed every 3–4 days. After 10–14 days, the organoids were removed from the Matrigel, mechanically dissociated into small fragments, and then split 1:4–1:6 in fresh Matrigel, enabling the formation of new organoids. All cell cultures were routinely tested for mycoplasma contamination by quantitative reverse transcription–polymerase chain reaction (qRT-PCR).

2.2. hAO characterization

Total RNA from organoids was isolated using TRIzol reagent, according to the manufacturer's instructions. The RNA concentration and purity were verified using a NanoDrop ND-100 spectrophotometer (NanoDrop Technologies). For the qRT-PCR assay, cDNA was synthesised from 200 ng of total RNA with SuperScript IV VILO. The cDNA was diluted 10-fold, and 1 μL of the sample was used as a template for qRT-PCR analysis with SYBR Select Master Mix on a CFX96 thermal cycler (Bio-Rad). The relative expression levels of the specific target genes, taken from an airway organoid milestone paper (Sachs et al., 2019), were determined using the $\Delta\Delta C_t$ method and normalized to the geometric mean of the ACTB and TBP mRNA levels using the primers listed in Table S2.

To characterize the hAO, gene expression analysis by qRT-PCR was performed after 10–14 days of standard culture and again after MPF exposure to investigate possible changes in the lung cell compartments: Claudin 1 (CLDN1) for lung epithelium, Keratin 5 (KRT5) for basal cells, NK2 Homeobox 1 (NKX2.1) for lung cell marker, Nephrocystin 1 (NPHP1) and Dynein Axonemal Heavy Chain 5 (DNAH5) for ciliated cells, Secretoglobin Family 1A member 1 (SCGB1A1) for club cells, Surfactant protein A1 (SFTPA1) and Surfactant protein C (SFTPC) for Alveolar Type 2 (AT2) cells. All primers were reported in Table S2.

2.3. Sampling and characterization of MPFs from a dryer machine

To generate environmentally relevant MPFs for the human organoid exposure experiment, polyester fibers emitted from the drying of synthetic clothes and fabrics were collected. Specifically, one polyester t-shirt, six sweatshirts, and two blankets of different colors (dry weight: 5427 g) were washed in a washing machine and subsequently dried in a common domestic tumble dryer. The dryer filter was previously cleaned by a vacuum cleaner, and all fibers derived from the first drying cycle were discarded. The same items were then washed again, and the synthetic fibers from the filtered exhaust air of the tumble dryer were collected (Figure S1), wrapped in aluminum foil, and transported to the laboratory for subsequent analyses.

The MPFs were first morphologically analyzed with a Leica EZ4D stereomicroscope and then with a Leica DMRA2 light microscope equipped with a Leica DC300 F digital camera. The size distribution, detailed morphology, and the elemental composition (C:O ratio) of the fibers were studied with a Zeiss LEO 1430 scanning electron microscope (SEM) coupled with a Centaurus detector for energy dispersive x-ray spectroscopy (EDS) analysis. A subsample of MPFs was mounted onto standard SEM stubs and gold-coated. For the size distribution analysis, thirty SEM images (magnification × 50) were taken. The length (n = 450) and width (n = 450) of MPFs was measured with the imaging software ImageJ. The width of the irregular fibers (e.g. flat fibers) was measured at their smallest and largest width in equal numbers. The elemental analysis was performed using Oxford Instruments INCA version 4.04 software (Abingdon, UK). The operating conditions were as follows: accelerating voltage, 20 kV; probe current, 360 pA; and working distance, 15.0 mm.

To further characterize the material, attenuated total reflection Fourier transform infrared spectroscopy (ATR-FTIR) on bulk polyester fabrics was performed using a Perkin Elmer FTIR Spectrometer Spectrum One and a Perkin Elmer Universal ATR Sampling Accessory consisting of a diamond crystal. Measurements were carried out in a wavenumber range of 4000–650 cm^{-1} with a spectral resolution of 4 cm^{-1}.

2.4. MPF exposure to hAOs

The MPFs collected from the filter of the dryer machine were resuspended at a final concentration of 500 μg mL^{-1} in AdDMEM/F12 supplemented with 10 mM Hepes, 1 × penicillin/streptomycin, and 1 × Glutamax; then the sample was sonicated at a high intensity (3 × 5 min) using a Bioruptor sonicator (Diagenode). To obtain organoid-MPF co-cultures, the hAOs were split as described above, and then the organoid fragments were embedded in Matrigel drops and mixed with MPFs at a ratio of 70% Matrigel with organoids and 30% culture medium containing the MPFs, at different concentrations (1, 10, and 50 μg mL^{-1}). Differently from Watson et al. (2016), who used inverted monolayers to assure that polypropylene nanoplastics contacted the cell surfaces, the here performed fragmentation allowed the outer as well as the inner cell surface of the organoid to have contact with the MPF. Moreover, to improve the exposure, we removed the organoids from the Matrigel, allowing them to grew in culture suspension. So far, the organoids showed an apical-out polarity as previously reported (Co et al., 2019), improving their barrier function against external stimuli. Upon solidification of the Matrigel, the organoid-MPF coculture was supplemented again with the culture medium containing the MPFs at the respective concentrations. After ten days, the organoids reached maturation (ca. 200–300 μm in diameter). At this point, in order to improve the interaction between the organoids and MPFs, the hAOs were carefully removed from the Matrigel and cultured in suspension with only culture medium containing the MPFs at the same concentrations for 1 week with gentle agitation. An organoid coculture was cultivated under the same conditions without MPF exposure as a control. After exposure, the airway organoid-MPF cocultures were collected for gene expression analysis and fixed for confocal microscopy and SEM analysis, as described below.

2.5. SEM analysis

To study the effects of MPFs on organoid growth, the control and exposed samples were fixed in a mixture of 4% paraformaldehyde and 2% glutaraldehyde in 0.1 M sodium cacodylate-buffered solution at pH 7.4. After several washes in the same buffer, the samples were post-fixed in 1% OsO_4 for 1.5 h at 4 °C and then dehydrated in a graded ethanol series. As a final step, the organoids were treated with hexamethyldisilazane for complete chemical dehydration. All samples were mounted onto standard aluminum stubs, gold sputtered, and analyzed under a Zeiss LEO 1430 SEM at 20 kV.

2.6. Immunofluorescence staining and confocal microscopy

For confocal microscopy analysis, the organoids were washed with 0.01 M phosphate-buffered saline, pH 7.4 (PBS) and fixed for 15 min in 4% paraformaldehyde, incubated in 0.05 M NH_4Cl in PBS for 30 min, permeabilized for 15 min in PBS containing 1% bovine serum albumin (BSA) and 0.2% Triton X-100, and blocked for 30 min in 1% BSA. The organoids were incubated overnight at 4 °C with a mouse monoclonal antibody against α-tubulin diluted in 0.1% BSA/PBS. The samples were then rinsed in PBS and incubated for 3 h at room temperature with rhodamine phalloidin (cytoskeleton) and the secondary Alexa Fluor 488-conjugated goat anti-mouse antibody. After several washes with PBS, the organoids were finally incubated for 5 min at room temperature with the DNA dye Hoechst 33342 (1:5000). At the end of the staining

procedure, the organoids were washed with PBS (3 × 5 min), mounted in 1:2 PBS/glycerol, and observed under a Nikon A1 confocal microscope.

For the images in Fig. 1 showing the immunofluorescent sections of the hAOs, the organoids were fixed 2 °C in PBS containing 0.2% Triton X-100, 5% BSA, 2% FBS and 5% goat serum. For the staining, the organoids were incubated O/N at 4 °C with the specific primary antibody in PBS containing 0.2% Triton X-100, 3% BSA and 3% FBS. After

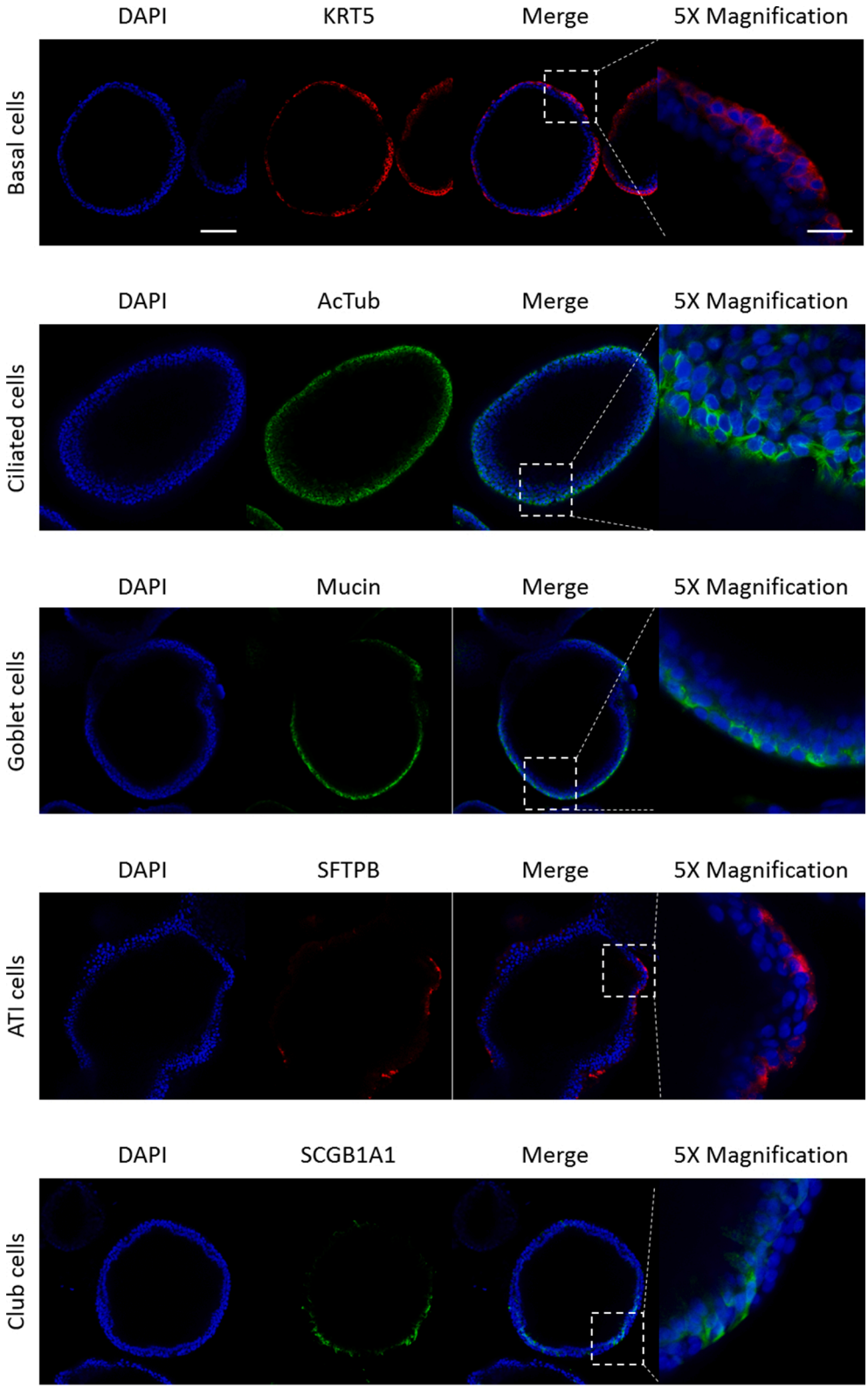

Fig. 1. Organoids recapitulate human airway counterpart. Immunofluorescent sections of human airway organoids (hAOs) showing markers for basal cells (KRT5), ciliated cells (acetylated α-tubulin), goblet cells (Mucin), ATI cells (SFTPB) and club cells (SCGB1A1). Nuclei were counterstained in blue. Scale bars: 100 μm, 25 μm (inset × 5 magnification). (For interpretation of the references to color in this figure legend, the reader is referred to the web version of this article.)

five washes with PBS containing 0.05% Triton X-100, the organoids were incubated O/N at 4 °C with specific conjugated secondary antibodies. Finally, nuclei were stained O/N at 4 °C with DAPI. Images were acquired using a Leica TCS SP8 confocal microscope (Leica, Wetzlar, Germany) with HC Pl fluotar APO 20x/0.55 objective.

2.7. Inflammatory cytokine, oxidative stress and obesogenic evaluation

To investigate the possible changes in the inflammatory cytokine expression in hAOs after MPF exposure, gene expression analysis by qRT-PCR was performed as described above at the end of the coculture with the highest MPF concentration using the primers listed in Table S2. Considering that the exposure of MPFs could induce oxidative stress in human tissues (Hu and Palić, 2020), we analyzed the expression of genes involved in oxidative stress pathways reported in relation to MPF exposure, including superoxide dismutase family genes (SOD1 and SOD2), glutathione detox-related genes (GSTA1 and GPX1), catalase (CAT), and ROS-controlling genes (NOX2, COX1, and ND1). In addition, the capacity of our 3D structures to respond to standard inflammatory stimuli was evaluated after treatment with poly(I:C) (50 μg mL^{-1}) or Staphylococcal enterotoxin B (SEB, 2 μg mL^{-1}) as a positive control.

To investigate a possible contribution of MPF to obesogenic effects (Kannan and Vimalkumar, 2021), gene expression analysis by qRT-PCR was performed as previously described. We analyzed the following genes involved in the adipogenic pathway: peroxisome proliferator-activated receptor gamma (PPARγ), a transcription factor that induces the adipogenic gene expression program during development, promotes adipose remodeling, and regulates the functions of adipocytes in lipid storage, adipokine secretion, and energy homeostasis, and its associated adiponectin.

For the ELISA analysis, organoids supernatant was collected and centrifuged at 300 × g for 5 min. Interleukin-6 concentration was determined using ultra-sensitive ELISA kit (Immunotools, Germany) according to the manufacturer's instructions.

For the flow cytometry analysis, hAOs were collected and washed with PBS and centrifuged for 10 min at 300 × g. Then, cells were dissociated by trypsinization using Trypsin with EDTA for 30 min to obtain a single-cell suspension. The samples were stained using 1:200 MitoSOX red mitochondrial superoxide indicator (Table S1), and incubated for 20 min in the dark at room temperature (RT). Finally, the samples were suspended in PBS and analysed using the FACSCanto II cytometer with FACSDiva analysis software (BD).

2.8. Organoid volume measurement

To determine the volume of hAOs, bright-field images were acquired with a Nikon Eclipse TS100 microscope equipped with a digital camera (Nikon Instrument Europe) at the end of the MPF exposure. hAOs (n = 10 fields) were analyzed at × 4 magnification. At least three independent experiments were analyzed. Organoid volumes were calculated in ImageJ software using the following formula: $4/3\,\pi\,r^3$, where "r" was the mean of the longest diameter and the shortest diameter of the spheroid divided by two.

2.9. MTT test

The hAOs (control groups and MPFs-treated groups) were seeded as previously described and at the end of the MPFs exposure they were collected and used for the MTT assay as described below. First, hAOs were washed with PBS to remove all the culture medium and successively seeded into non-tissue culture 24-well plates with a phenol red free DMEM high glucose medium containing the MTT substrate. After a 2 h incubation at 37 °C the medium was replaced with a 96% ethanol and all the samples were incubated for 1 h at 37 °C in dark. Finally, all the ethanol containing the product of MTT reaction was collected and its absorbance was detected using a spectrophotometer (TECAN, GENios plus) at 570 nm.

2.10. Data analysis

For statistical analysis of the gene expression data, a two-way analysis of variance followed by Bonferroni's multiple comparison test ($\alpha = 0.05$) was performed. The metabolic activity was tested by *t*-test analysis followed by Kolmogorov-Smirnov correction. Photoshop was used to export the image graphs.

3. Results

3.1. hAO isolation and characterization

The hAOs were generated starting from biopsies of healthy lung donors. When embedded in Matrigel, lung cells were organized in a polarized pseudostratified epithelium with a central hollow lumen, resulting positive for basal (KRT5), ciliated (AC-TUB), goblet (Mucin), ATI (SFTPB) and club (SCGB1A1) cell markers, supporting their airway identity (Fig. 1). Gene expression analysis showed that the hAO lines derived from three different donors have similar gene expression profiles recapitulating all cell types of airway tissue (compared to human pancreas organoids as a control), supporting the reproducibility of our culture methods (Figure S2).

The organoids were analyzed by optical microscopy, confocal 3D construction, and SEM imaging. The normal organoids (control group) exhibited a spherical shape with a typical diameter of 200–300 μm and an inner cavity (Fig. 2A–B). Confocal 3D reconstruction confirmed that the cells were well differentiated, showing the presence of ciliated cells and nonciliated cells, including club cells (identified by the presence of microvilli), that were irregularly distributed on the surface and corresponding to their *in vivo* position (Fig. 2C–E). Immunofluorescence experiments with the actin cytoskeleton marker revealed the different shapes and dimensions of the cells containing nuclei, which were visible in the surface section (Fig. 2C–E) and transverse plane (Fig. 2D). Moreover, the inner surface of the organoids established a differentiated cell structure, including ciliated cells facing the organoid cavity, as demonstrated in Fig. 2D. The presence of cilia at the inner surface of the organoids could be explained by the rotating motion of the organoid cavity, which can be seen in a video recording of the organoids (Video S1). Finally, high-resolution SEM imaging of the organoid surface showed the same irregularly shaped ciliated and nonciliated cells, displaying the dimensions of the cilia and microvilli (Fig. 2F).

3.2. MPFs in the air filter of a dryer machine

The total weight of the MPFs removed from the air filter of a dryer machine was 2.3 g (Figure S1), which was released from 5.4 kg of 100% polyester fabrics. The procedure was repeated once again with the same fabrics (rewashing and redrying), and the release of MPFs was 2.5 g (0.44 g ± 0.014 of dry MPFs kg^{-1} dry fabric, 1 SD, $n = 2$). Optical microscopy experiments demonstrated fibers of different colors, reflecting the color mixture of the dried materials (Fig. 3A–B). For a more detailed analysis, SEM (Fig. 3C–E) revealed that the MPFs varied in size and morphology. The fiber length was on average 700 ± 400 μm (1 SD, $n = 450$, min 68 μm, max 3,638 μm). The size distribution analysis (Fig. 3F) showed that the majority of fibers were in the range of 200–800 μm (68.5 %). Only 5.6 % of MPFs were smaller than 200 μm, and 0.4 % larger than 2,200 μm. Interestingly, the shape of these MPFs differed at the transverse surface; no MPFs had a round profile along the entire length, but they exhibited a varying profile from flat and twisted to tattered (Fig. 3C–E). Flat MPFs exhibited maximum widths of 25 μm along their widest dimension and a minimum height of 1 μm along their thinnest dimension. The fiber width was on average 10 ± 5 μm (1 SD, $n = 450$). Furthermore, we observed that some fibers showed a rough surface, where small pieces of < 10 μm flaked off from the fiber (Fig. 3D)

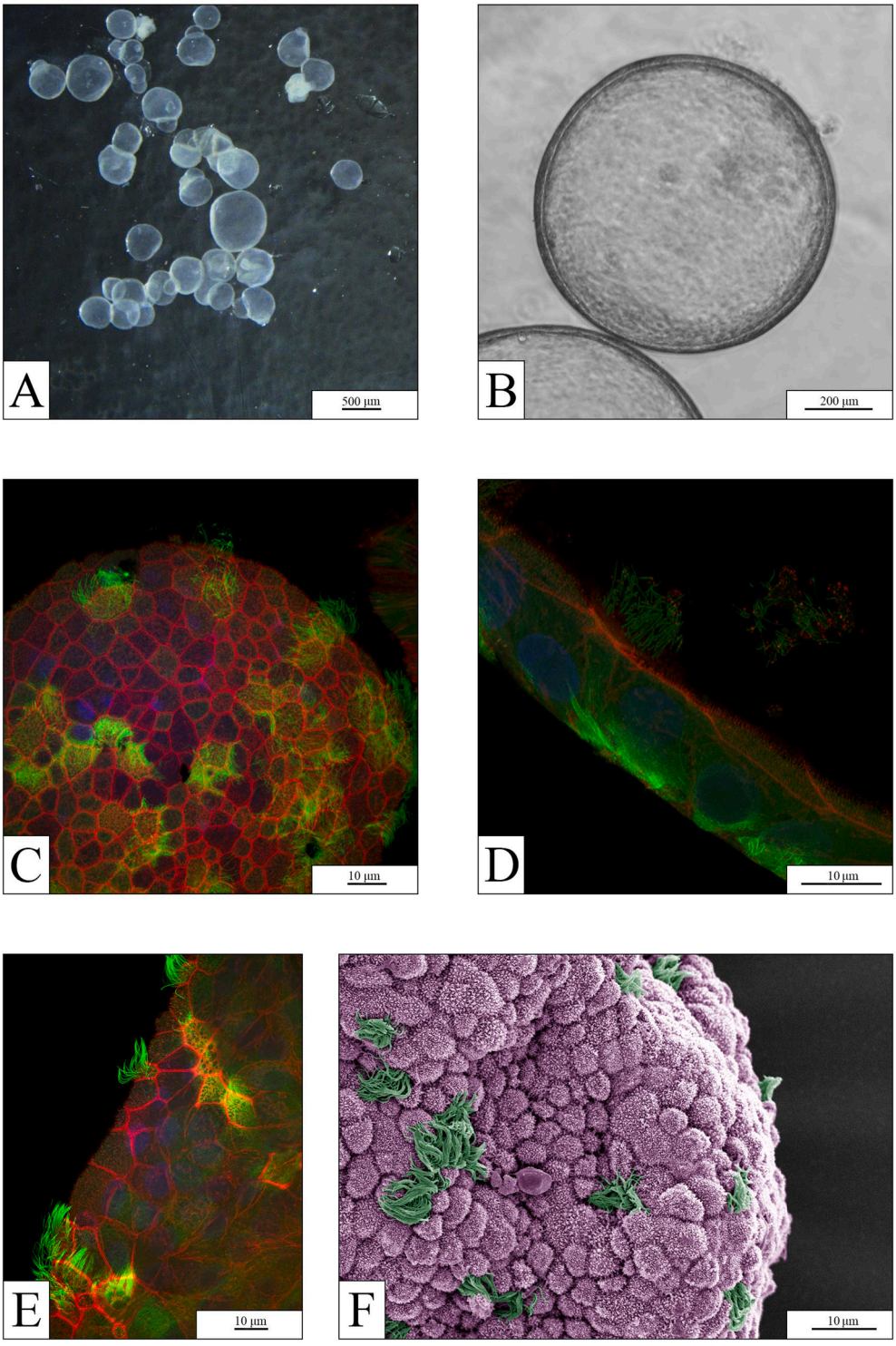

Fig. 2. Characterization of human airway organoids (control group, $n = 3$). (A) Stereo microscopy image and (B) optical microscopy image of organoids. (C–E) Immunofluorescence imaging of the organoid surface and the transverse section generated by confocal microscopy showing the cellular organization with a cytoskeletal marker (anti-acetylated tubulin; green) and counterstaining of the actin cytoskeleton (phalloidin 565; red) and nuclei (Hoechst 33342; blue). (F) Pseudo-colored SEM image of the organoid's surface showing irregularly shaped multiciliated (green) and nonciliated cells with microvilli (purple). (For interpretation of the references to color in this figure legend, the reader is referred to the web version of this article.)

or a chapped ending was revealed (Fig. 3E), which could lead to the release of very small MPs from the fibers.

Although very speculative, we estimated the number of fibers released by the drying process by considering the average dimensions of the fibers and their uncertainties (SE of the mean). From the mean measured dimensions of collected fibers and the propagation of their errors, we determined a fiber volume of $V_{fiber} = 7.0 \times 10^{-5} \pm 5.2 \times 10^{-6}$ mm^3 $fiber^{-1}$ ($\pm\delta V_{fiber}$) and an average mass of a fiber of $M_{fiber} = 9.6 \times 10^{-5} \pm 7.2 \times 10^{-6}$ mg $fiber^{-1}$ ($\pm\delta M_{fiber}$), assuming that the density of polyester is 1.38 mg mm^{-3} and that the density's variability was negligible in comparison to that of the fiber volume. According to these data, 2.3 g of polyester fibers collected in the filter of a dryer machine should contain $23 \times 10^6 \pm 1.7 \times 10^6$ fibers. Given the large SD of measured fiber length and width and the resulting large uncertainty of the fiber volume and mass, the calculated values (number of fibers) also had large variability. Nevertheless, the estimate provides an order of magnitude for the number of fibers that could be released from the drying of synthetic fabrics.

Elemental analysis of single fibers isolated from the dryer lint showed a C:O ratio of 74:26, which corresponds to that of polyester (see

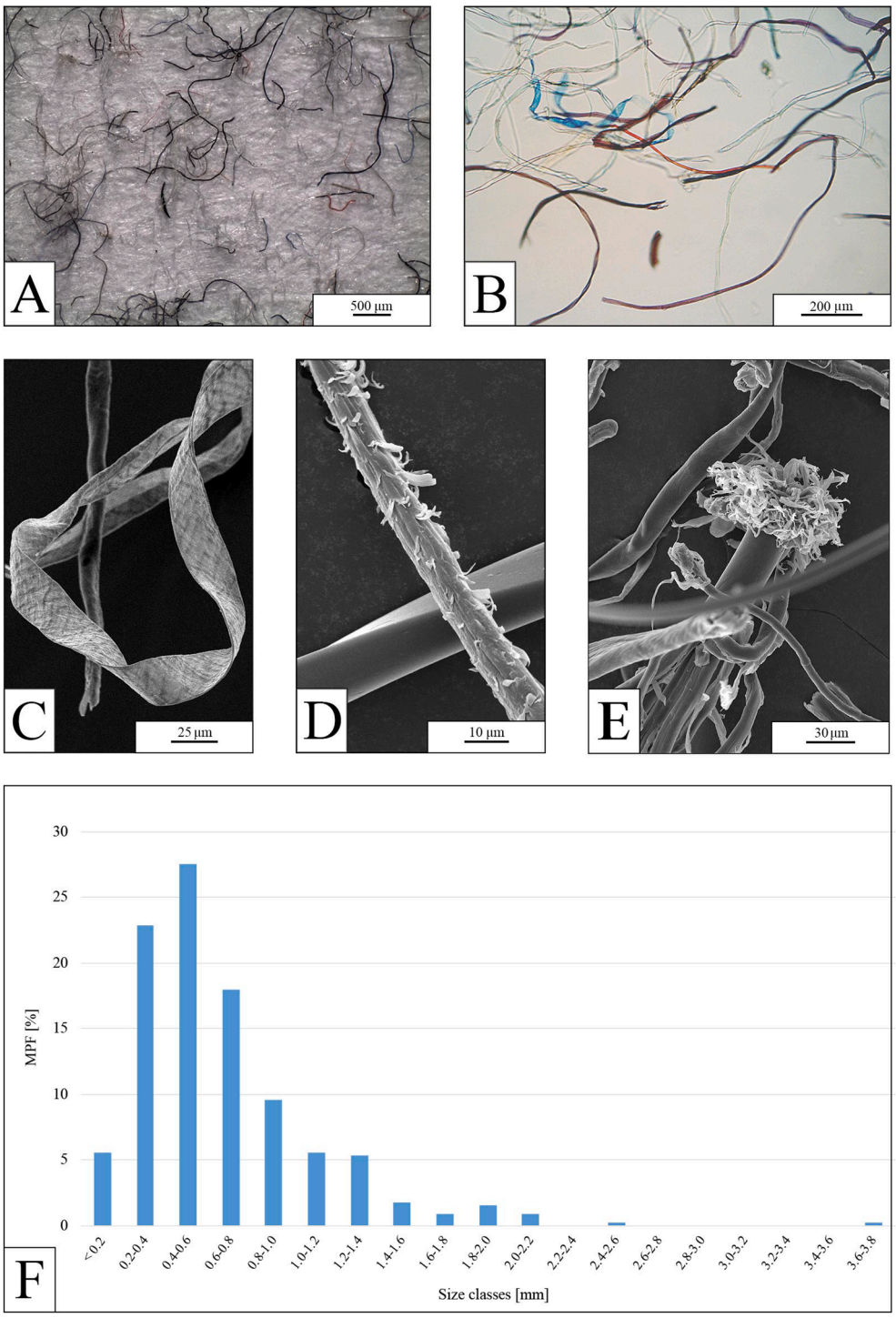

Fig. 3. Synthetic fibers obtained from the air filter of a dryer machine. (A–B) Optical microscopy images demonstrating MPFs of different sizes and colors. (C–E) SEM images of MPFs at different magnifications showing varying morphologies. (F) Size distribution analysis of $n = 450$ MPFs, number percentages are grouped in 200 µm size classes.

Figure S3 for the EDS spectrum). The ATR-FTIR spectrum of all original bulk fabrics used for the drying showed all characteristic absorbance peaks of polyester (Figure S4, ATR-FTIR spectrum of PET from a plastic water bottle as reference).

3.3. hAOs exposed to MPFs

The hAOs exposed to MPFs were affected by all concentrations of MPFs. Based on the average mass of a fiber and the suspension volume in the exposure wells (0.5 mL), we estimate the number concentrations of MPFs which were added to the organoid cultures to be 5 ± 1, 52 ± 4, and 259 ± 19 MPFs well^{-1}. Optical microscopy, confocal 3D construction, and SEM image analyses revealed that the organoids exposed to MPFs were not inhibited in their growth and did not exhibit any cellular abnormalities compared to the control group, independent of the MPF concentration (Fig. 4A–F). Most organoids did not interact with the fibers, or only to a small extent, and maintained their radial (almost spherical) architecture (Fig. 4D–F).

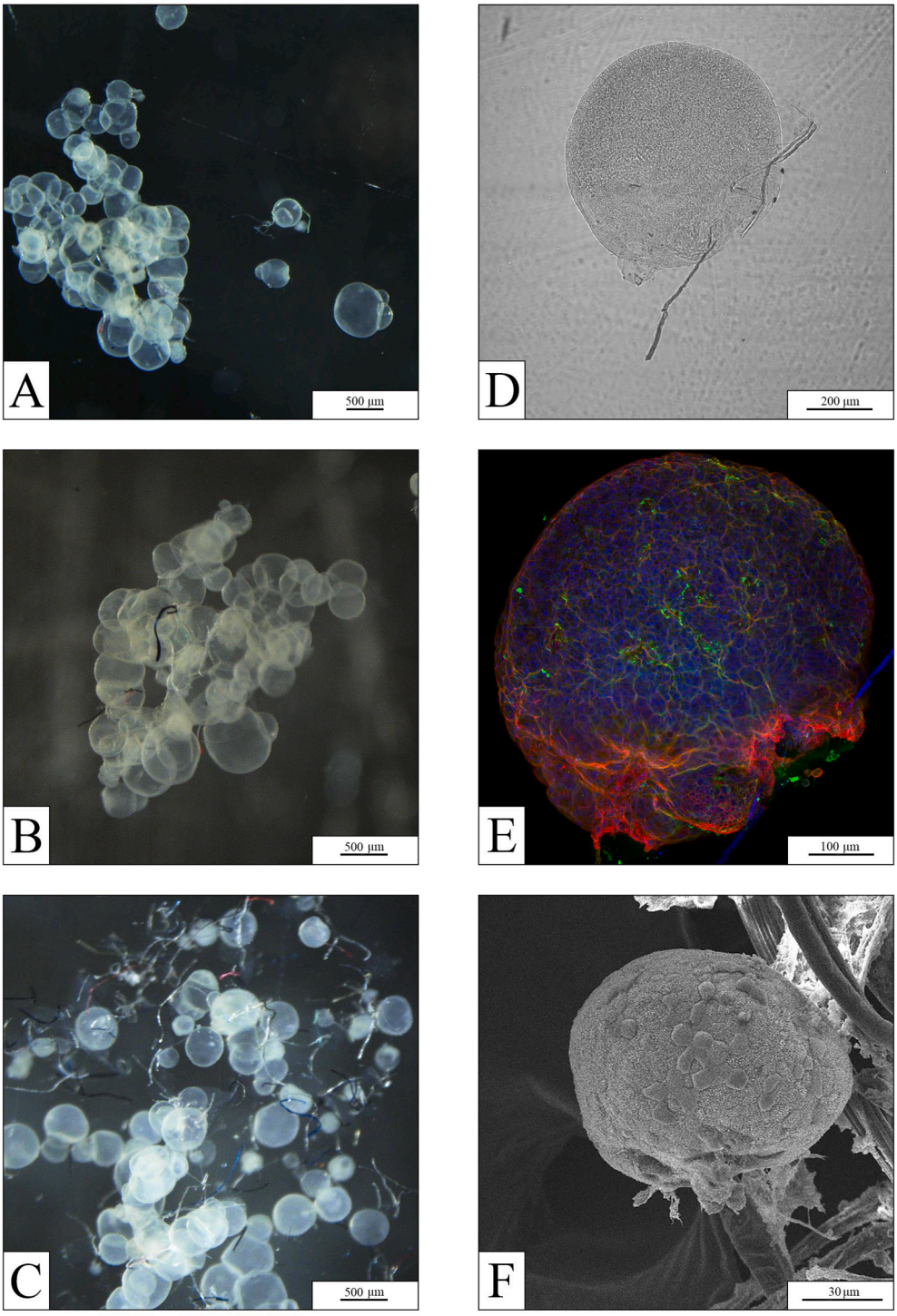

Fig. 4. MPFs interact with hAOs in coculture. (A–C) Stereo microscopy images of organoids in suspension with MPFs at increasing concentrations (top to bottom: 1, 10, and 50 µg mL^{-1}). (D) Phase contrast image and (E) immunolabeled 3D reconstruction of the same organoid (MPF concentration: 10 µg mL^{-1}) showing the interaction between the organoid and a fiber. The organoid was stained for cytoskeletal proteins: microtubules (anti-acetylated tubulin; green), F-actin (phalloidin 565; red), and nuclei (Hoechst 33342; blue). Also visible in blue is a synthetic fiber. (F) SEM image of an organoid (MPF concentration: 50 µg mL^{-1}) in contact with a fiber, demonstrating a spherical body and a differentiated cell structure. All analyses were performed at least three times. (For interpretation of the references to color in this figure legend, the reader is referred to the web version of this article.)

Fluorescence staining of the surface (Fig. 5A–B) and transverse (Fig. 5C) sections of the organoids as well as high-resolution SEM images (Fig. 5D–H) showed the same cellular structure as the controls, including ciliated and nonciliated cells, even when the organoids were in contact with MPFs. The notable observation was a higher density of polarization of the cytoskeleton near the fiber contact site, visible as an intensification of the red color in Fig. 5B. Owing to an organoid that had broken apart (likely during the transfer of the dehydrated organoid onto the aluminum stub), we were able to take SEM images of the inner surface of the organoids and could observe the same cellular differentiation (multiciliated and nonciliated cells) as the outer surface (Fig. 5E). Rather than depending on the MPF concentration, the observed effects varied with the degree of MPF-organoid contact, which presumably depended on the development phase of the organoids. The organoids that made contact with fibers during maturation grew around the fibers (Fig. 5F–H). No assumptions could be made on a size-dependent effect of the MPFs as the experimental setup did not account for this. All effects are attributed to the size ranges mentioned before.

Interestingly, the organoids closely bonded to an MPF formed an organoid-fiber interlacement or fully encompassed the MPF. We further observed that some organoids grew polarized around the fibers. For example, Fig. 6A–G shows cell growth along the length of a fiber. The

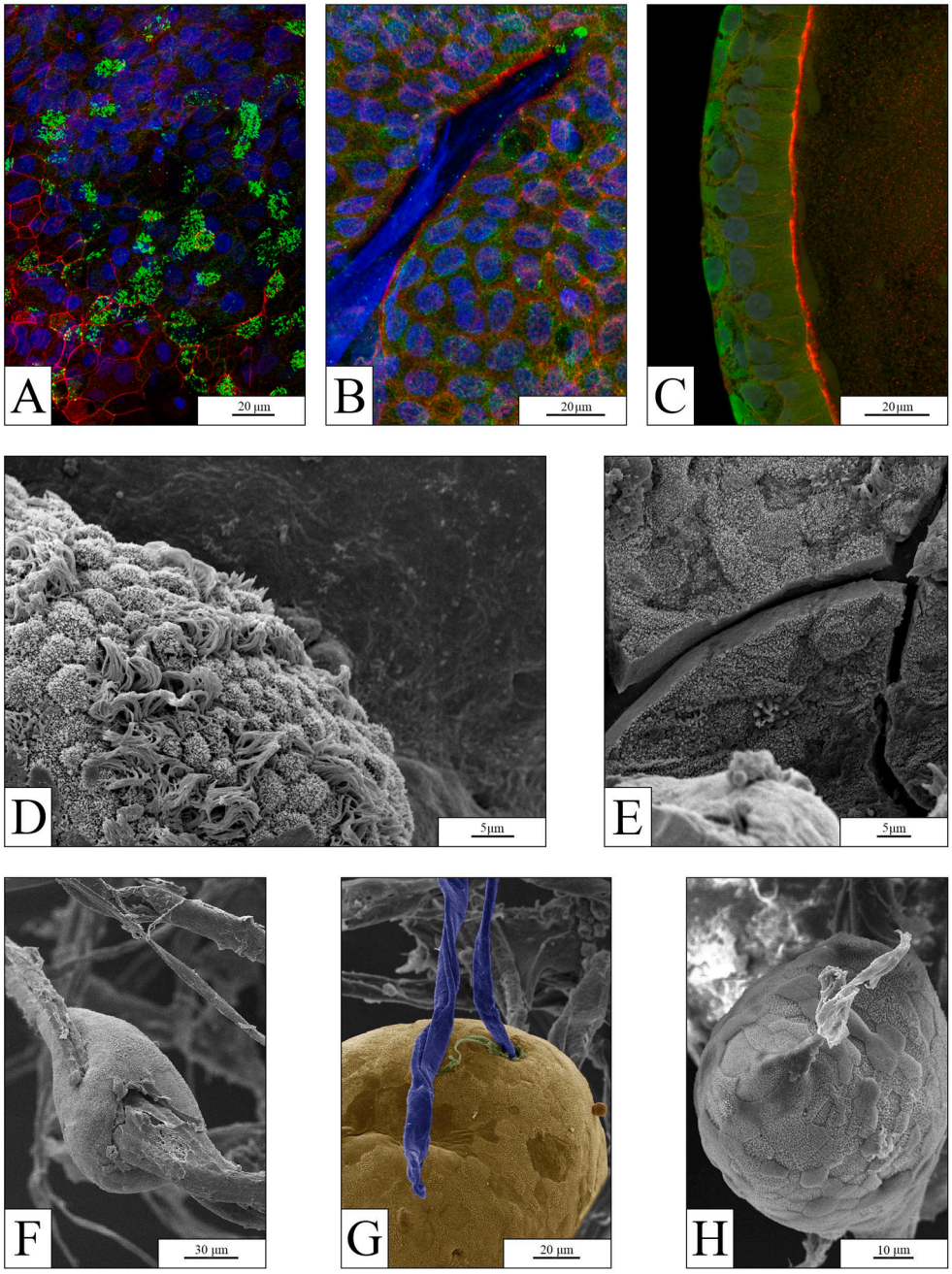

Fig. 5. hAOs growth around the fibers. (A–B) Surface and (C) transverse sections of an immunolabeled organoid (MPF concentration: 50 µg mL^{-1}) showing the cell organization. The organoid was stained to show ciliated cells (anti-acetylated tubulin; green), F-actin cytoskeleton (phalloidin 565; red), and nuclei (Hoechst 33342; blue). Also visible in blue is a synthetic fiber. (D) SEM image of an organoid's outer surface showing ciliated and nonciliated cells (MPF concentration: 10 µg mL^{-1}). (E) SEM image of the inner surface of an organoid that had broken apart, demonstrating cell differentiation facing the organoid's cavity (MPF concentration: 10 µg mL^{-1}). (F–H) SEM images of organoids (MPF concentration: 50 µg mL^{-1}) demonstrating a differentiated cell structure and integration of a fiber into the organoid; the image in panel G is partially pseudo-colored for better visualization (cell tissue, yellow; fiber, blue). All analyses were performed at least three times. (For interpretation of the references to color in this figure legend, the reader is referred to the web version of this article.)

organoids seemingly surrounded the fibers by developing netlike extensions of cells (clearly visible in Fig. 6D–F), resulting in a full internalization of the MPFs. While the cells of the organoid body growing along the length of a fiber exhibited a differentiated structure (Fig. 6A–B), the thin cell extension covering the surface of a fiber exiting the organoid body (Fig. 6D–F) was rather smooth and uniform. These observations of cells covering a fiber with a thin layer stands in contrast to the images depicted in Fig. 5F–H showing that cells did not cover the fibers once they left the organoid. We also noticed that organoids in suspension with MPFs can be damaged by fibers piercing the cell tissue (Fig. 6C).

3.4. Effect of MPF on hAOs

To verify that the lung heritage of hAOs was not affected by their exposure to MPFs, we performed gene expression analysis of the typical epithelial lung markers NKX2.1 and CLDN1 as well as the specific airway lung markers SFTPA1 and SFTPC (AT2 cells), SCGB1A1 (club cells), NPHP1 and DNAH5 (ciliated cells), and KRT5 (basal cells); all these genes were slightly reduced even if not at a statistically significant level except for the SCBG1A1 that was significantly less expressed (Fig. 7A). In addition, no difference in the expression of epithelial to mesenchymal transition markers was observed (Fig. 7B).

Regarding the possible obesogenic effects associated to MPF exposure as recently suggested by Kannan and Vimalkumar (2021), we observed a slight increase in hAO volume relevance after MPF treatment. However, this tendency was not significant as also showed by gene expression analysis of genes involved in the adipogenic pathway (Fig. 7C–D). MTT viability test showed no significant differences between the control group and the MPFs treated group of hAO (Figure S5A).

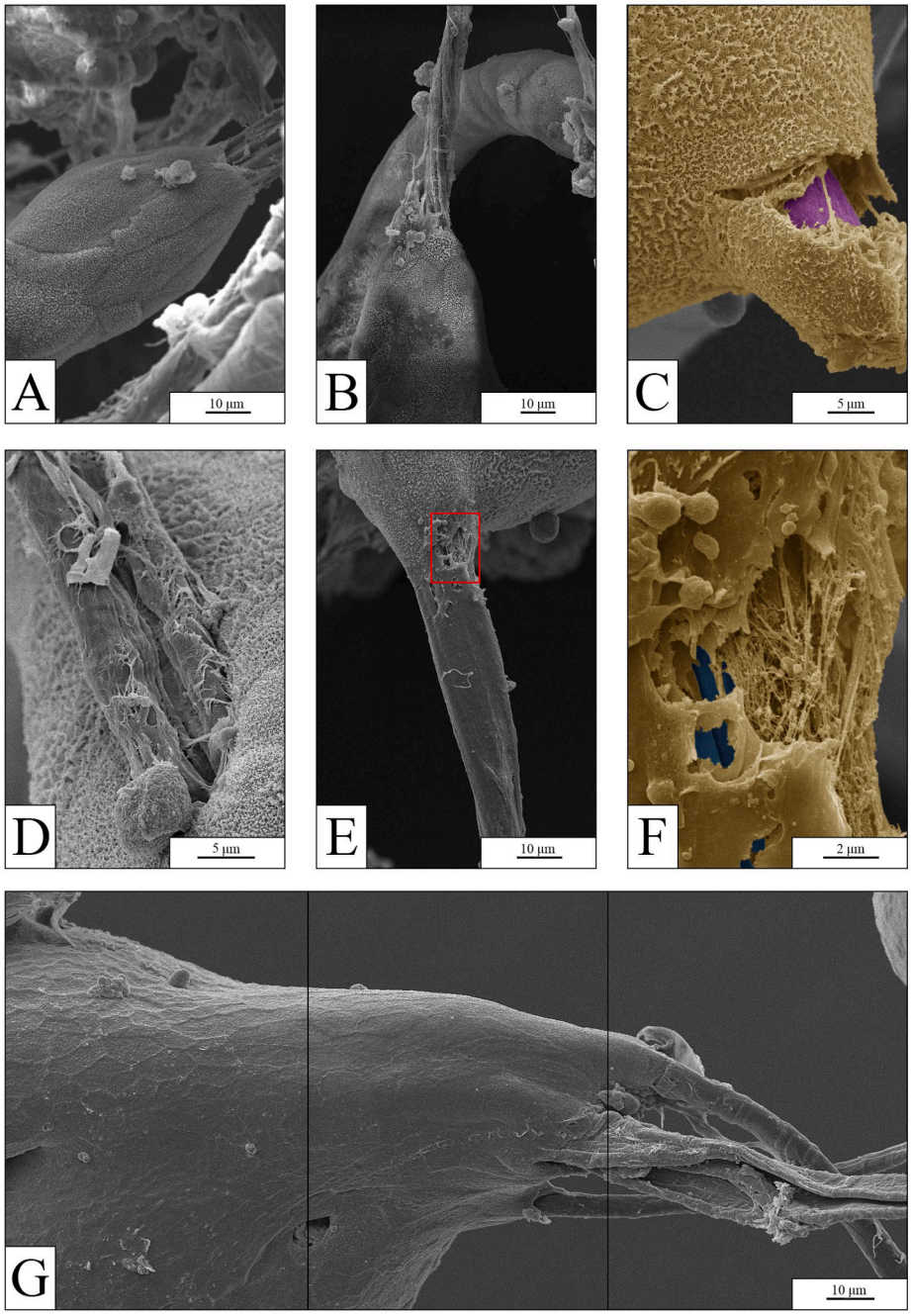

Fig. 6. SEM images of hAOs exposed to MPFs. Partially pseudo-colored for better visualization (cell tissue, yellow; fibers, purple/blue). (A–B) Oriented cell growth of organoids along the length of a fiber; the cell structure and partially coated fibers are shown (MPF concentration: 10 µg mL^{-1}). (C) Complete internalization of a fiber inside an organoid (MPF concentration: 50 µg mL^{-1}). (D) Net-like extension of cells growing on a fiber. (E and its magnification F) Thin cell extension covering the surface of a fiber exiting the organoid body (MPF concentration: 50 µg mL^{-1}). (G) Merged image of three continuous images showing the polarized growth of organoids with the length of multiple fibers (MPF concentration: 50 µg mL^{-1}). All analyses were performed at least three times. (For interpretation of the references to color in this figure legend, the reader is referred to the web version of this article.)

3.5. *Inflammation and oxidative stress evaluation*

To investigate possible changes in the expression of inflammatory cytokines and oxidative stress-related genes, gene expression analysis of hAOs was performed at the end of their coculture with the highest MPF concentration. The results revealed no significant differences in the gene expression of cytokines or oxidative stress-related genes (Fig. 8A–B), while GSTA1 and COX1 showed a slight increase in hAOs exposed to MPFs in relation to the control hAOs (Fig. 8B). In contrast, an increase of inflammatory markers was observed after xenobiotic stimuli, as observed in other organoid models (Aguilar et al., 2021, Jose et al., 2020) (Fig. 8A). Focusing on the protein level, IL 6 was not observed in the medium of hAOs treated with microplastics, while an increase amount of this cytokine was detected after xenobiotic treatment (Figure S5B). Regarding the mitochondrial oxidative stress, hAOs exposed to MPFs and to poly(I:C) showed a similar trend of oxidative stress, as also observed in 2D cell culture and animal model (Dong et al., 2020; Ruenraroengsak and Tetley, 2015; Umamaheswari et al., 2021) but only with the positive control the level of mitochondrial superoxide was statistically significant versus the non-treated hAOs (Figure S5C).

4. Discussion

The first objective of the present study was to set up an innovative *in vitro* model based on the use of 3D structures that could adequately represent the native lung, where emerging atmospheric contaminants such as synthetic materials could have adverse human health effects. And secondly, we wanted to use this model to investigate the potential effects of polyester fibers isolated from a dryer machine on human lung biology, most of all after the recent evidences showing that even the

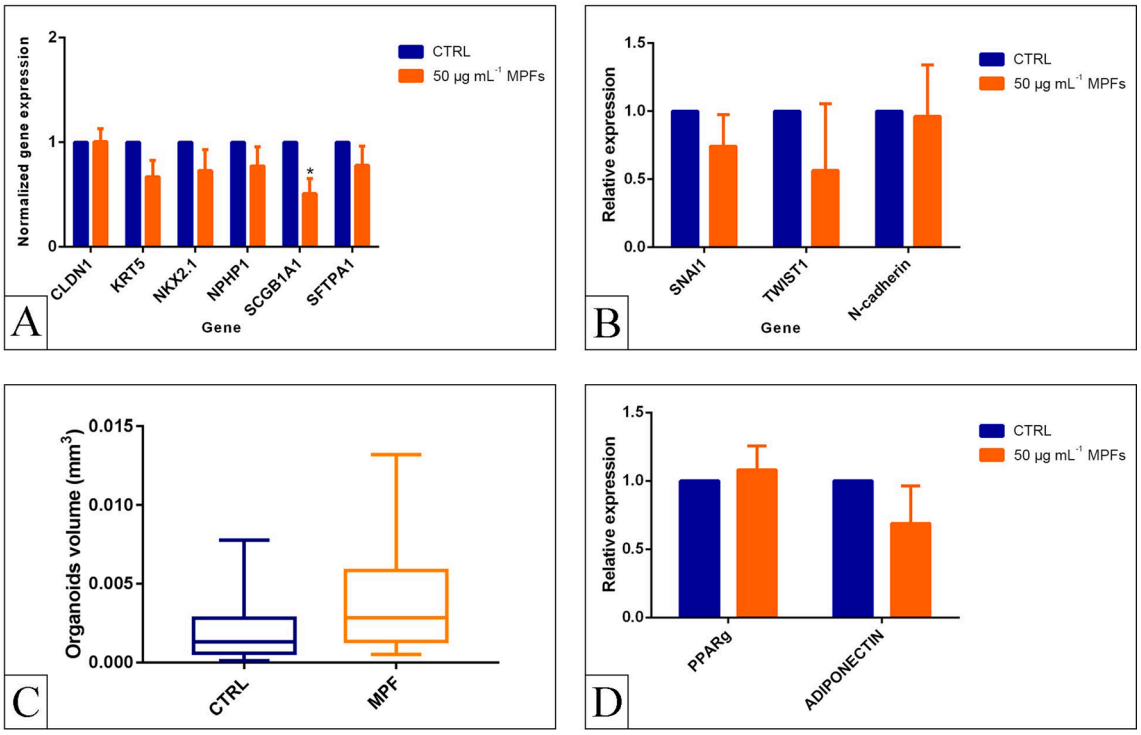

Fig. 7. hAOs were not affected by MPFs. Control organoids compared to organoids exposed to MPFs (MPF concentration: 50 µg mL^{-1}) for selected target genes: (A) general epithelial lung markers and specific airway markers, (B) epithelial to mesenchymal transition markers, (C) organoid volume calculated measuring their long and short diameter ($n = 3$). (D) qRT-PCR analysis of the control organoids compared to organoids exposed to MPFs (MPF concentration: 50 µg mL^{-1}) for adipogenic target genes. Data in panel A, B, D are shown as means ± S.E.M. ($n = 4$), statistical analysis was performed by two-way ANOVA followed by Bonferroni correction; * $P < 0.05$. Data in panel C are shown as box and whisker plot; the line within the box marks the median, the boundaries of the boxes the 25 and 75 percentiles, and the whisker limits delineate the minimum and the maximum value after outlier removal.

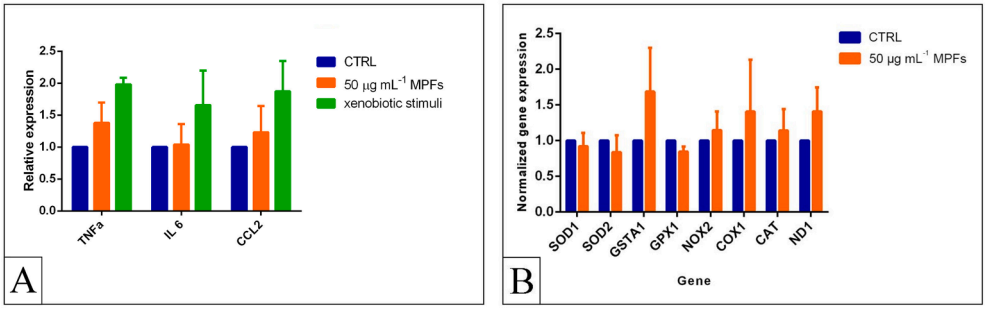

Fig. 8. qRT-PCR analysis for inflammation and oxidative stress evaluation. Control organoids compared to organoids exposed to MPFs (MPF concentration: 50 µg mL^{-1}) for selected target genes: (A) Inflammatory cytokines compared to the response of positive control organoids to standard inflammatory stimuli, and (B) oxidative stress-related genes. Data are shown as means ± S.E.M. ($n = 4$), statistical analysis was performed by two-way ANOVA followed by Bonferroni correction.

emissions of MPFs from mechanical drying are found in the air, particularly indoor air (O'Brien et al., 2020).

It is becoming increasingly clear that the 3D cell culture is a more accurate way to represent human tissue outside the body and simulate conditions in a living organism. Standard 2D cell cultures (monolayers), with cells often all at the same stage, cannot accurately represent how cells grow or how they are affected by disease and injury (Jensen and Teng, 2020). In this context, organoids have been recently exploited to overcome the limitations of 2D cell culture systems. Due to their capacity to self-organize into minimal biological units and thus potentially recapitulate the functionality and complexity of the tissue of origin, they have emerged as powerful models for studying human development and disease (Fatehullah et al., 2016). Although airway organoids do not yet recapitulate all of the complex structures and cellular interactions associated with the different regions of the lung (e.g., trachea, bronchi, bronchioles, alveoli and all mesenchymal and vascular compartments), they contain the specific cell types present in the epithelium of the original organ. Therefore, they can be applied for basic and translational research (Barkauskas et al., 2017). We showed that lung-specific cell types, including basal, AT2, and ciliated cells, are represented in our human airway organoids (Fig. 5A).

To date organoids derived from different sources have been used to successfully study specific diseases (Dutta et al., 2017; Mellin and Boddey, 2020) and to screen new drugs (Broutier et al., 2017). Already some studies have been published to support how these three-dimensional structures provide a new opportunity to mimic human organ development, morphology and physiology in a similar manner as *in vivo* models (Lancaster et al., 2013; Schutgens and Clevers, 2020). In this panorama, human lung organoids have been used to mimic a response to inflammatory stimuli (Jose et al., 2020) and to study the

pathophysiology of *Cryptosporidium* infection (Heo et al., 2018). The compatibility of this system for the toxicological assessment has been recently reported by Truskey (2018) and by Kuratnik and Giardina (2013).

This study presents an attempt to use human airway organoids for the assessment of the effects of MPFs. Although plastics are inert materials, in recent years several studies have described health risks for humans through the many routes of MPF exposure. Not least, the recent increased use of synthetic masks due to the COVID-19 pandemic exacerbated for example the route of inhalation. Despite the existing knowledge about MPs, less is known regarding the MPF particulate toxicity effects in a short- and long-term exposure and still many mechanisms have to be elucidated regarding their impact on human health.

Synthetic textiles have been identified and extensively described as one of the major sources of MPFs in wastewater (Browne et al., 2011; De Falco et al., 2019). The current research is the first to report the amount and features of MPFs released from synthetic fabrics in a dryer machine, addressing potential atmospheric contamination. In fact, a recent paper by O'Brien et al. (2020) has shown that the use of dryer machines causes an increase of the MPF concentration in the ambient air; however, they did not measure the total amount of MPFs released by the drying process. Washing and drying textiles in household machines present two possible MPF emission pathways: one being through the wastewater (residual water in textiles after the centrifugation cycle of the washing machine), and one being via the air passing by an integrated air filter. The former goes directly into domestic wastewater without filters. Here, we focused on the air pathway; MPFs released by textiles and forced by a strong air flux into the air exhaust are retained by the air filter and then specifically collected at the end of each drying cycle. Considering the evidence reported by O'Brien et al. (2020), the air filter does not remove all MPFs coming from the dryer machine. Thus, the total amount of MPFs released in the air flux can be even higher. FTIR analysis showed clean spectra for bulk fabric confirming polyester material (Figure S4).

Based on a review of studies regarding atmospheric MPs, Prata et al. (2020a; 2020b) calculated that a person's lungs could be exposed to 26–130 airborne MPs a day. This estimation is slightly lower than the average inhaled concentration of 272 MPs per day determined by Vianello et al. (2019). The effects of MPs on human health have been previously tested only using a variety of 2D cell lines (Dong et al., 2020; Hwang et al., 2019; Palaniappan et al., 2021; Schirinzi et al., 2017). The observed effects were very diverse and depended on the properties of the particle (e.g., size and polymer), the duration and concentration of exposure (6-12-24-48 h), and the tested cell lines. In particular, tests representing the human lung should use MPs in size and shape that have been shown to be present in the air. Since a substantial portion of airborne environmental MPs consists mostly of MPFs between 200 and 600 μm (Dris et al., 2016; Henry et al., 2019) and fibers greater than 250 μm have been found in human lungs (Pauly et al., 1998), the MPFs applied in the current study (51% having sizes between 200 and 600 μm) represent an environmentally relevant and realistic test material.

Our experimental MPF concentrations (with an estimated 518 MPFs mL^{-1}, corresponding to 50 μg mL^{-1}) are in agreement with previously published studies on 2D methodology (Dong et al., 2020; Hwang et al., 2019). Moreover, in the hAO exposure volume of 0.5 mL (single well volume where organoids were incubated), the mass and estimated number of MPFs were 0.5 μg and 5 MPFs, 5 μg and 52 MPFs, and 25 μg and 259 MPFs, for the three concentrations, respectively. For the purpose of this experiment, which was to determine the effect on hAOs once in contact with the fibers, we focused on the direct points of contact rather than on the overall fitness of the hAOs in the well (e.g. a counting of intact hAOs per well). Indeed, the first step of most of the inhaled particles, including MPFs is the deposition by impaction (Vianello et al., 2019). Therefore, this organoid-MPF contact situation triggered the interaction between fibers and lung epithelium once fibers reach the inner lung tissues, independently from their concentrations in the air.

Our findings show that after an MPF exposure of 17 days, only a slight non-statistically significant increase in the expression of the inflammatory markers both at molecular and protein level was observed. Potential toxic effects attributable to MPs observed in exposed animal models include impairment of adipogenesis and lipid metabolism (Kannan and Vimalkumar, 2021; Lu et al., 2018). Therefore, we investigated two crucial key regulators of metabolism, PPARγ and adiponectin (Astapova and Leff, 2012), but no statistically significant changes were observed. Organoid volumes at the end of the MPF exposure showed a slight but still evident increase (Fig. 7C). Overall, no clear obesity-promoting effect can be determined after our MPF exposure.

The airway epithelium is the first barrier of the host defense system in the respiratory tract. An adequate and balanced cell composition guarantees an optimal epithelial structure and functionality. In respiratory diseases, this balance may be altered. In our experiments, we observed a change in this cellular balance but most relevant is that SCGB1A1 was found to be significantly reduced. This club cell secretory protein is mainly expressed by nonciliated respiratory epithelial cells and has demonstrated potent anti-inflammatory, anti-tumor, and antitoxicant functions (Broeckaert and Bernard, 2000; Lakind et al., 2007). SCGB1A1 has frequently been used as a biomarker to monitor lung injury caused by various diseases or environmental exposures. Its decrease has been consistently observed to associate with airway inflammatory diseases (Broeckaert et al., 2006; Zhu et al., 2019).

Confocal microscopy and SEM images did not provide any evidence of organoid cell growth inhibition. This observation was not completely surprising, as the field of biomaterials is increasingly demonstrating how plastic can be applied as an inert scaffold to support cell growth for human tissue engineering without altering the biological features (Jubeli et al., 2019). Although the biocompatibility of several plastic materials has already been demonstrated (the hAO themselves grew inside plastic wells made of polystyrene, control included), polyester fibers can contain additives that can be added to textiles in order to impart desirable physical, chemical, and biological (i.e., antimicrobial, color) properties (Chu et al., 2021; Sait et al., 2021). Since additives are typically not covalently bonded to the polymer matrix and can therefore leach, they are considered more harmful than the polymer itself, inducing several effects such as endocrine disruption, immunotoxicity (Tang et al., 2020), genotoxicity and developmental toxicity (Zhao et al., 2020). Our results did not show significant inflammation- or oxidative stress-induced effects of polyester MPFs on hAO development, suggesting that additives, whenever they were present, did not cause adverse effects. However, any further conclusions about long-term effects cannot be drawn with this model.

One of the most relevant results related to MPF exposure was the polarization of the cell growth along the fibers such that the organoid was induced to envelop the encountered fibers by a cellular layer. This behavior was clearly observed in different cases and at different MPF concentrations, indicating that it should be carefully considered a possible adverse effect of MPFs. This effect is particularly alarming if we consider repair processes that could follow MPF inhalation, as it is known that fibers can be retained in the lungs.

If we compare our 3D *in vitro* experimental approach with the already published 2D experimental strategies, we have to underline that our system has been exposed to MPFs for a longer period of time, 17 days versus 6–24 h (Dong et al., 2020; Hwang et al., 2019; Palaniappan et al., 2021; Schirinzi et al., 2017). The longer exposure time could explain the slight differences observed where our hAO had enough time to adapt to the MP environment. The presented data, which combine morphological approaches with molecular/biochemical techniques, were suitable to characterize the MPFs-hAO interactions from a complementary perspective; while confocal and electron microscopy were able to evaluate the overall results on organoid morphology and architecture also at cellular level, the added toxicological markers analyzed three specific toxicological pathways in more detail: inflammation, oxidative stress, and obesogenic response. However, further insights are needed to

complete the toxicological analysis of MPFs. A more detailed analysis could include a co-localization analysis of MPF, changes in specific cell markers, levels of key enzymes which control the anti-oxidative balance, such as superoxide dismutase (SOD), or the contents of other oxidative stress marker, such as malondialdehyde (MDA). These methodologies are suggestions for further evaluation of the effects of airborne pollutants such as MPFs on humans and to further test the proposed human exposure model.

5. Conclusion

In the present study, we employed a 3D *in vitro* model representing a normal lung to test the effects of inhaled and deposited MPFs. Based on the findings of this study, the presence of nonbiodegradable fibers during the repair phase of a damaged lung epithelium may lead to their inclusion in the repaired tissue with unknown effects on long term perspective. Moreover, we observed a significant reduction of SCGB1A1 gene expression, which has frequently been used as a biomarker to monitor lung injury. Having thoroughly described the cell composition of the hAOs used for the first time via gene expression and microscopic analyses, this work contributes to the development of urgently needed human models for assessing the impact of particulate matter pollutants. We conclude that hAOs are suitable for testing MPs and other airborne contaminants, including NPs, to determine the potential risks of atmospheric particles in developing adverse pulmonary effects, but further testing is needed to yield valuable insights using this model and complete the analysis of the effects of inhaled MPFs.

6. Author Information

Lorenza Lazzari is co-last author for the human organoids. Renato Bacchetta is co-last-author for microplastic and microscopy analyses.

Funding

This research did not receive any specific grant from funding agencies in the public, commercial, or not-for-profit sectors.

CRediT authorship contribution statement

Anna Sophie Winkler: Formal analysis, Writing – original draft, Writing – review & editing, Visualization. **Alessandro Cherubini:** Formal analysis, Investigation, Writing – review & editing. **Francesco Rusconi:** Formal analysis, Investigation, Writing – review & editing. **Nadia Santo:** Investigation. **Laura Madaschi:** Investigation. **Clelia Pistoni:** Investigation. **Giorgia Moschetti:** Investigation. **Maria Lucia Sarnicola:** Investigation. **Mariacristina Crosti:** Investigation. **Lorenzo Rosso:** Investigation. **Paolo Tremolada:** Conceptualization, Methodology, Formal analysis, Resources, Writing – review & editing. **Lorenza Lazzari:** Writing – review & editing, Methodology, Resources, Investigation, Supervision. **Renato Bacchetta:** Conceptualization, Methodology, Investigation, Resources, Writing – review & editing, Visualization, Supervision.

Declaration of Competing Interest

The authors declare that they have no known competing financial interests or personal relationships that could have appeared to influence the work reported in this paper.

Acknowledgements

We appreciated Dr. Elena Pini from the Department of Pharmaceutical Sciences at the University of Milan for performing the FTIR analyses. The authors would like to thank Dr. Angela Ronchi for her inspiration.

Appendix A. Supplementary material

Supplementary data to this article can be found online at https://doi.org/10.1016/j.envint.2022.107200.

References

Aguilar, C., Alves da Silva, M., Saraiva, M., Neyazi, M., Olsson, I.A.S., Bartfeld, S., 2021. Organoids as host models for infection biology – a review of methods. Exp. Mol. Med. 53 (10), 1471–1482. https://doi.org/10.1038/s12276-021-00629-4.

Akanyange, S.N., Lyu, X., Zhao, X., Li, X., Zhang, Y., Crittenden, J.C., Anning, C., Chen, T., Jiang, T., Zhao, H., 2021. Does microplastic really represent a threat? A review of the atmospheric contamination sources and potential impacts. Sci. Total Environ. 777, 146020. https://doi.org/10.1016/j.scitotenv.2021.146020.

Ambrosini, R., Azzoni, R.S., Pittino, F., Diolaiuti, G., Franzetti, A., Parolini, M., 2019. First evidence of microplastic contamination in the supraglacial debris of an alpine glacier. Environ. Pollut. 253, 297–301. https://doi.org/10.1016/j.envpol.2019.07.005.

Astapova, O., Leff, T., 2012. Adiponectin and PPARγ, in: Vitamins & Hormones. Elsevier, pp. 143–162. https://doi.org/10.1016/B978-0-12-398313-8.00006-3.

Barkauskas, C.E., Chung, M.-I., Fioret, B., Gao, X., Katsura, H., Hogan, B.L.M., 2017. Lung organoids: current uses and future promise. Development 144, 986–997. https://doi.org/10.1242/dev.140103.

Barshtein, G., Livshits, L., Shvartsman, L.D., Shlomai, N.O., Yedgar, S., Arbell, D., 2016. Polystyrene nanoparticles activate erythrocyte aggregation and adhesion to endothelial cells. Cell Biochem. Biophys. 74 (1), 19–27. https://doi.org/10.1007/s12013-015-0705-6.

Bergmann, M., Wirzberger, V., Krumpen, T., Lorenz, C., Primpke, S., Tekman, M.B., Gerdts, G., 2017. High Quantities of microplastic in arctic deep-sea sediments from the HAUSGARTEN observatory. Environ. Sci. Technol. 51 (19), 11000–11010. https://doi.org/10.1021/acs.est.7b0333110.1021/acs.est.7b03331.s001.

Bhagat, J., Zang, L., Nishimura, N., Shimada, Y., 2020. Zebrafish: an emerging model to study microplastic and nanoplastic toxicity. Sci. Total Environ. 728, 138707. https://doi.org/10.1016/j.scitotenv.2020.138707.

Broeckaert, Bernard, 2000. Clara cell secretory protein (CC16): characteristics and perspectives as lung peripheral biomarker: Clara cell secretory protein. Clin. Exp. Allergy 30 (4), 469–475. https://doi.org/10.1046/j.1365-2222.2000.00760.x.

Broeckaert, F., Clippe, A., Knoops, B., Hermans, C., Bernard, A., 2006. Clara cell secretory protein (CC16): features as a peripheral lung biomarker. Ann. N. Y. Acad. Sci. 923, 68–77. https://doi.org/10.1111/j.1749-6632.2000.tb05520.x.

Broutier, L., Mastrogiovanni, G., Verstegen, M.MA., Francies, H.E., Gavarró, L.M., Bradshaw, C.R., Allen, G.E., Arnes-Benito, R., Sidorova, O., Gaspersz, M.P., Georgakopoulos, N., Koo, B.-K., Dietmann, S., Davies, S.E., Praseedom, R.K., Lieshout, R., IJzermans, J.N.M., Wigmore, S.J., Saeb-Parsy, K., Garnett, M.J., van der Laan, L.JW., Huch, M., 2017. Human primary liver cancer-derived organoid cultures for disease modeling and drug screening. Nat. Med. 23 (12), 1424–1435. https://doi.org/10.1038/nm.4438.

Browne, M.A., Crump, P., Niven, S.J., Teuten, E., Tonkin, A., Galloway, T.S., Thompson, R.C., 2011. Accumulation of microplastic on shorelines wordwide: sources and sinks. Environ. Sci. Technol. 9175–9179 https://doi.org/10.1021/es201811s.

Bruinink, A., Wang, J., Wick, P., 2015. Effect of particle agglomeration in nanotoxicology. Arch. Toxicol. 89 (5), 659–675. https://doi.org/10.1007/s00204-015-1460-6.

Chu, J., Hu, X., Kong, L., Wang, N., Zhang, S., He, M., Ouyang, W., Liu, X., Lin, C., 2021. Dynamic flow and pollution of antimony from polyethylene terephthalate (PET) fibers in China. Sci. Total Environ. 771, 144643. https://doi.org/10.1016/j.scitotenv.2020.144643.

Churg, A., Bauer, M., 2000. Ambient atmospheric particles in the airways of human lungs. Ultrastruct. Pathol. 24, 353–361. https://doi.org/10.1080/019131200750060014.

Co, J.Y., Margalef-Català, M., Li, X., Mah, A.T., Kuo, C.J., Monack, D.M., Amieva, M.R., 2019. Controlling epithelial polarity: a human enteroid model for host-pathogen interactions. Cell Rep. 26 (9), 2509–2520.e4. https://doi.org/10.1016/j.celrep.2019.01.108.

Cortés, C., Domenech, J., Salazar, M., Pastor, S., Marcos, R., Hernández, A., 2020. Nanoplastics as a potential environmental health factor: effects of polystyrene nanoparticles on human intestinal epithelial Caco-2 cells. Environ. Sci. Nano 7 (1), 272–285. https://doi.org/10.1039/C9EN00523D.

Costa, E.C., Moreira, A.F., de Melo-Diogo, D., Gaspar, V.M., Carvalho, M.P., Correia, I.J., 2016. 3D tumor spheroids: an overview on the tools and techniques used for their analysis. Biotechnol. Adv. 34 (8), 1427–1441. https://doi.org/10.1016/j.biotechadv.2016.11.002.

De Falco, F., Di Pace, E., Cocca, M., Avella, M., 2019. The contribution of washing processes of synthetic clothes to microplastic pollution. Sci. Rep. 9, 6633. https://doi.org/10.1038/s41598-019-43023-x.

De Felice, B., Bacchetta, R., Santo, N., Tremolada, P., Parolini, M., 2018. Polystyrene microplastics did not affect body growth and swimming activity in Xenopus laevis tadpoles. Environ. Sci. Pollut. Res. 25 (34), 34644–34651. https://doi.org/10.1007/s11356-018-3408-x.

Domenech, J., Hernández, A., Rubio, L., Marcos, R., Cortés, C., 2020. Interactions of polystyrene nanoplastics with in vitro models of the human intestinal barrier. Arch. Toxicol. 94 (9), 2997–3012. https://doi.org/10.1007/s00204-020-02805-3.

Dong, C.-D., Chen, C.-W., Chen, Y.-C., Chen, H.-H., Lee, J.-S., Lin, C.-H., 2020. Polystyrene microplastic particles: in vitro pulmonary toxicity assessment. J. Hazard. Mater. 385, 121575. https://doi.org/10.1016/j.jhazmat.2019.121575.

Dossena, M., Piras, R., Cherubini, A., Barilani, M., Dugnani, E., Salanitro, F., Moreth, T., Pampaloni, F., Piemonti, L., Lazzari, L., 2020. Standardized GMP-compliant scalable production of human pancreas organoids. Stem Cell Res. Ther. 11, 94. https://doi.org/10.1186/s13287-020-1585-2.

Dris, R., Gasperi, J., Mirande, C., Mandin, C., Guerrouache, M., Langlois, V., Tassin, B., 2017. A first overview of textile fibers, including microplastics, in indoor and outdoor environments. Environ. Pollut. 221, 453–458. https://doi.org/10.1016/j.envpol.2016.12.013.

Dris, R., Gasperi, J., Saad, M., Mirande, C., Tassin, B., 2016. Synthetic fibers in atmospheric fallout: A source of microplastics in the environment? Mar. Pollut. Bull. 104 (1-2), 290–293. https://doi.org/10.1016/j.marpolbul.2016.01.006.

Dutta, D., Heo, I., Clevers, H., 2017. Disease modeling in stem cell-derived 3D organoid systems. Trends Mol. Med. 23 (5), 393–410. https://doi.org/10.1016/j.molmed.2017.02.007.

Fatehullah, A., Tan, S.H., Barker, N., 2016. Organoids as an in vitro model of human development and disease. Nat. Cell Biol. 18 (3), 246–254. https://doi.org/10.1038/ncb3312.

Gaston, E., Woo, M., Steele, C., Sukumaran, S., Anderson, S., 2020. Microplastics differ between indoor and outdoor air masses: insights from multiple microscopy methodologies. Appl. Spectrosc. 74 (9), 1079–1098.

Goldberg, M.S., Thériault, G., 1994. Retrospective cohort study of workers of a synthetic textiles plant in Quebec: I. General mortality. Am. J. Ind. Med. 25 (6), 889–907. https://doi.org/10.1002/ajim.4700250612.

Henry, B., Laitala, K., Klepp, I.G., 2019. Microfibres from apparel and home textiles: prospects for including microplastics in environmental sustainability assessment. Sci. Total Environ. 652, 483–494. https://doi.org/10.1016/j.scitotenv.2018.10.166.

Heo, I., Dutta, D., Schaefer, D.A., Iakobachvili, N., Artegiani, B., Sachs, N., Boonekamp, K.E., Bowden, G., Hendrickx, A.P.A., Willems, R.J.L., Peters, P.J., Riggs, M.W., O'Connor, R., Clevers, H., 2018. Modelling cryptosporidium infection in human small intestinal and lung organoids. Nat. Microbiol. 3 (7), 814–823. https://doi.org/10.1038/s41564-018-0177-8.

Hu, M., Palić, D., 2020. Micro- and nano-plastics activation of oxidative and inflammatory adverse outcome pathways. Redox Biol. 37, 101620. https://doi.org/10.1016/j.redox.2020.101620.

Huch, M., Gehart, H., van Boxtel, R., Hamer, K., Blokzijl, F., Verstegen, M.A., Ellis, E., van Wenum, M., Fuchs, S., de Ligt, J., van de Wetering, M., Sasaki, N., Boers, S., Kemperman, H., de Jonge, J., Ijzermans, J.M., Nieuwenhuis, E.S., Hoekstra, R., Strom, S., Vries, R.G., van der Laan, L.W., Cuppen, E., Clevers, H., 2015. Long-term culture of genome-stable bipotent stem cells from adult human liver. Cell 160 (1-2), 299–312. https://doi.org/10.1016/j.cell.2014.11.050.

Hwang, J., Choi, D., Han, S., Choi, J., Hong, J., 2019. An assessment of the toxicity of polypropylene microplastics in human derived cells. Sci. Total Environ. 684, 657–669. https://doi.org/10.1016/j.scitotenv.2019.05.071.

Jensen, C., Teng, Y., 2020. Is it time to start transitioning from 2D to 3D cell culture? Front. Mol. Biosci. 7, 33. https://doi.org/10.3389/fmolb.2020.00033.

Jose, S.S., De Zuani, M., Tidu, F., Hortová Kohoutková, M., Pazzagli, L., Forte, G., Spaccapelo, R., Zelante, T., Frič, J., 2020. Comparison of two human organoid models of lung and intestinal inflammation reveals toll-like receptor signalling activation and monocyte recruitment. Clin. Transl. Immunol. 9 (5) https://doi.org/10.1002/cti2.v9.510.1002/cti2.1131.

Jubeli, E., Khzam, A., Yagoubi, N., 2019. Cells integration onto scaffolds prepared from polyester based polymers – importance of polymer thermal properties in addition to hydrophilicity. Int. J. Polym. Mater. Polym. Biomater. 68 (17), 1068–1077. https://doi.org/10.1080/00914037.2018.1525549.

Kämpfer, A.A.M., Busch, M., Schins, R.P.F., 2020. Advanced *in vitro* testing strategies and models of the intestine for nanosafety research. Chem. Res. Toxicol. 33 (5), 1163–1178. https://doi.org/10.1021/acs.chemrestox.0c00079.

Kannan, K., Vimalkumar, K., 2021. A review of human exposure to microplastics and insights into microplastics as obesogens. Front. Endocrinol. 12, 724989 https://doi.org/10.3389/fendo.2021.724989.

Kapp, K.J., Miller, R.Z., Mukherjee, A., 2020. Electric clothes dryers: an underestimated source of microfiber pollution. PLoS ONE 15 (10), e0239165. https://doi.org/10.1371/journal.pone.0239165.

Kuratnik, A., Giardina, C., 2013. Intestinal organoids as tissue surrogates for toxicological and pharmacological studies. Biochem. Pharmacol. 85 (12), 1721–1726. https://doi.org/10.1016/j.bcp.2013.04.016.

Lakind, J.S., Holgate, S.T., Ownby, D.R., Mansur, A.H., Helms, P.J., Pyatt, D., Hays, S.M., 2007. A critical review of the use of Clara cell secretory protein (CC16) as a biomarker of acute or chronic pulmonary effects. Biomarkers 12 (5), 445–467. https://doi.org/10.1080/13547500701359327.

Lancaster, M.A., Renner, M., Martin, C.-A., Wenzel, D., Bicknell, L.S., Hurles, M.E., Homfray, T., Penninger, J.M., Jackson, A.P., Knoblich, J.A., 2013. Cerebral organoids model human brain development and microcephaly. Nature 501 (7467), 373–379. https://doi.org/10.1038/nature12517.

Lim, S.L., Ng, C.T., Zou, L.i., Lu, Y., Chen, J., Bay, B.H., Shen, H.-M., Ong, C.N., 2019. Targeted metabolomics reveals differential biological effects of nanoplastics and nanoZnO in human lung cells. Nanotoxicology 13 (8), 1117–1132. https://doi.org/10.1080/17435390.2019.1640913.

Lippmann, M., Yeates, D.B., Albert, R.E., 1980. Deposition, retention, and clearance of inhaled particles. Occup. Environ. Med. 37 (4), 337–362. https://doi.org/10.1136/oem.37.4.337.

Liu, C., Li, J., Zhang, Y., Wang, L., Deng, J., Gao, Y., Yu, L., Zhang, J., Sun, H., 2019. Widespread distribution of PET and PC microplastics in dust in urban China and their estimated human exposure. Environ. Int. 128, 116–124. https://doi.org/10.1016/j.envint.2019.04.024.

Liu, L., Xu, K., Zhang, B., Ye, Y., Zhang, Q., Jiang, W., 2021. Cellular internalization and release of polystyrene microplastics and nanoplastics. Sci. Total Environ. 779, 146523. https://doi.org/10.1016/j.scitotenv.2021.146523.

Loomis, D., Grosse, Y., Lauby-Secretan, B., Ghissassi, F.E., Bouvard, V., Benbrahim-Tallaa, L., Guha, N., Baan, R., Mattock, H., Straif, K., 2013. The carcinogenicity of outdoor air pollution. Lancet Oncol. 14 (13), 1262–1263. https://doi.org/10.1016/S1470-2045(13)70487-X.

Lu, L., Wan, Z., Luo, T., Fu, Z., Jin, Y., 2018. Polystyrene microplastics induce gut microbiota dysbiosis and hepatic lipid metabolism disorder in mice. Sci. Total Environ. 631–632, 449–458. https://doi.org/10.1016/j.scitotenv.2018.03.051.

Lusher, A.L., Tirelli, V., O'Connor, I., Officer, R., 2015. Microplastics in arctic polar waters: the first reported values of particles in surface and sub-surface samples. Sci. Rep. 5, 14947. https://doi.org/10.1038/srep14947.

Mastrangelo, G., Fedeli, U., Fadda, E., Milan, G., Lange, J.H., 2002. Epidemiologic evidence of cancer risk in textile industry workers: a review and update. Toxicol. Ind. Health 18 (4), 171–181. https://doi.org/10.1191/0748233702th139rr.

Mellin, R., Boddey, J.A., 2020. Organoids for liver stage malaria research. Trends Parasitol. 36 (2), 158–169. https://doi.org/10.1016/j.pt.2019.12.003.

Nel, A., 2005. Air pollution-related illness: effects of particles. Science 308 (5723), 804–806.

O'Brien, S., Okoffo, E.D., O'Brien, J.W., Ribeiro, F., Wang, X., Wright, S.L., Samanipour, S., Rauert, C., Toapanta, T.Y.A., Albarracin, R., Thomas, K.V., 2020. Airborne emissions of microplastic fibres from domestic laundry dryers. Sci. Total Environ. 747, 141175. https://doi.org/10.1016/j.scitotenv.2020.141175.

Palaniappan, S., Sadacharan, C.M., Rostama, B., 2022. Polystyrene and polyethylene microplastics decrease cell viability and dysregulate inflammatory and oxidative stress markers of MDCK and L929 cells in vitro. Expo Health 14 (1), 75–85. https://doi.org/10.1007/s12403-021-00419-3.

Pauly, J.L., Stegmeier, S.J., Allaart, H.A., Cheney, R.T., Zhang, P.J., Mayer, A.G., Streck, R.J., 1998. Inhaled cellulosic and plastic fibers found in human lung tissue. Can. Epidemiol. Prev. Biomark. 7, 419–428.

Pimentel, J.C., Avila, R., Lourenco, A.G., 1975. Respiratory disease caused by synthetic fibres: a new occupational disease. Thorax 30 (2), 204–219. https://doi.org/10.1136/thx.30.2.204.

Prata, J.C., 2018. Airborne microplastics: consequences to human health? Environ. Pollut. 234, 115–126. https://doi.org/10.1016/j.envpol.2017.11.043.

Prata, J.C., Castro, J.L., da Costa, J.P., Cerqueira, M., Duarte, A.C., Rocha-Santos, T., 2020a. In: Handbook of Microplastics in the Environment. Springer International Publishing, Cham, pp. 1–25. https://doi.org/10.1007/978-3-030-10618-8_37-1.

Prata, J.C., da Costa, J.P., Lopes, I., Duarte, A.C., Rocha-Santos, T., 2020b. Environmental exposure to microplastics: an overview on possible human health effects. Sci. Total Environ. 702, 134455. https://doi.org/10.1016/j.scitotenv.2019.134455.

Reed, S., Clark, M., Thompson, R., Hughes, K.A., 2018. Microplastics in marine sediments near Rothera Research Station. Antarctica. Mar. Pollut. Bull. 133, 460–463. https://doi.org/10.1016/j.marpolbul.2018.05.068.

Rist, S., Carney Almroth, B., Hartmann, N.B., Karlsson, T.M., 2018. A critical perspective on early communications concerning human health aspects of microplastics. Sci. Total Environ. 626, 720–726. https://doi.org/10.1016/j.scitotenv.2018.01.092.

Ruenraroengsak, P., Tetley, T.D., 2015. Differential bioreactivity of neutral, cationic and anionic polystyrene nanoparticles with cells from the human alveolar compartment: robust response of alveolar type 1 epithelial cells. Part. Fibre Toxicol. 12, 19. https://doi.org/10.1186/s12989-015-0091-7.

Sachs, N., Papaspyropoulos, A., Zomer-van Ommen, D.D., Heo, I., Böttinger, L., Klay, D., Weeber, F., Huelsz-Prince, G., Iakobachvili, N., Amatngalim, G.D., de Ligt, J., van Hoeck, A., Proost, N., Viveen, M.C., Lyubimova, A., Teeven, L., Derakhshan, S., Korving, J., Begthel, H., Dekkers, J.F., Kumawat, K., Ramos, E., van Oosterhout, M. F., Offerhaus, G.J., Wiener, D.J., Olimpio, E.P., Dijkstra, K.K., Smit, E.F., van der Linden, M., Jaksani, S., van de Ven, M., Jonkers, J., Rios, A.C., Voest, E.E., van Moorsel, C.H., van der Ent, C.K., Cuppen, E., van Oudenaarden, A., Coenjaerts, F.E., Meyaard, L., Bont, L.J., Peters, P.J., Tans, S.J., van Zon, J.S., Boj, S.F., Vries, R.G., Beekman, J.M., Clevers, H., 2019. Long-term expanding human airway organoids for disease modeling. EMBO J. 38 https://doi.org/10.15252/embj.2018100300.

Sait, S.T.L., Sørensen, L., Kubowicz, S., Vike-Jonas, K., Gonzalez, S.V., Asimakopoulos, A. G., Booth, A.M., 2021. Microplastic fibres from synthetic textiles: Environmental degradation and additive chemical content. Environ. Pollut. 268, 115745. https://doi.org/10.1016/j.envpol.2020.115745.

Sato, T., Stange, D.E., Ferrante, M., Vries, R.G.J., van Es, J.H., van den Brink, S., van Houdt, W.J., Pronk, A., van Gorp, J., Siersema, P.D., Clevers, H., 2011. Long-term expansion of epithelial organoids from human colon, adenoma, adenocarcinoma, and Barrett's epithelium. Gastroenterology 141 (5), 1762–1772. https://doi.org/10.1053/j.gastro.2011.07.050.

Schirinzi, G.F., Pérez-Pomeda, I., Sanchís, J., Rossini, C., Farré, M., Barceló, D., 2017. Cytotoxic effects of commonly used nanomaterials and microplastics on cerebral and epithelial human cells. Environ. Res. 159, 579–587. https://doi.org/10.1016/j.envres.2017.08.043.

Schutgens, F., Clevers, H., 2020. Human organoids: tools for understanding biology and treating diseases. Annu. Rev. Pathol. 15 (1), 211–234. https://doi.org/10.1146/annurev-pathmechdis-012419-032611.

Shamir, E.R., Ewald, A.J., 2014. Three-dimensional organotypic culture: experimental models of mammalian biology and disease. Nat. Rev. Mol. Cell Biol. 15 (10), 647–664. https://doi.org/10.1038/nrm3873.

Takasato, M., Er, P.X., Chiu, H.S., Little, M.H., 2016. Generation of kidney organoids from human pluripotent stem cells. Nat. Protoc. 11 (9), 1681–1692. https://doi.org/10.1038/nprot.2016.098.

Tang, Y.u., Zhou, W., Sun, S., Du, X., Han, Y.u., Shi, W., Liu, G., 2020. Immunotoxicity and neurotoxicity of bisphenol A and microplastics alone or in combination to a bivalve species. Tegillarca granosa. Environ. Pollut. 265, 115115. https://doi.org/10.1016/j.envpol.2020.115115.

Triebskorn, R., Braunbeck, T., Grummt, T., Hanslik, L., Huppertsberg, S., Jekel, M., Knepper, T.P., Krais, S., Müller, Y.K., Pittroff, M., Ruhl, A.S., Schmieg, H., Schür, C., Strobel, C., Wagner, M., Zumbülte, N., Köhler, H.-R., 2019. Relevance of nano- and microplastics for freshwater ecosystems: a critical review. TrAC, Trends Anal. Chem. 110, 375–392. https://doi.org/10.1016/j.trac.2018.11.023.

Truskey, G.A., 2018. Human microphysiological systems and organoids as in vitro models for toxicological studies. Front. Public Health 6, 185. https://doi.org/10.3389/fpubh.2018.00185.

Tuveson, D., Clevers, H., 2019. Cancer modeling meets human organoid technology. Science 364 (6444), 952–955.

Umamaheswari, S., Priyadarshinee, S., Kadirvelu, K., Ramesh, M., 2021. Polystyrene microplastics induce apoptosis via ROS-mediated p53 signaling pathway in zebrafish. Chem. Biol. Interact. 345, 109550. https://doi.org/10.1016/j.cbi.2021.109550.

Valavanidis, Athanasios, Fiotakis, Konstantinos, Vlachogianni, Thomais, 2008. Airborne particulate matter and human health: toxicological assessment and importance of size and composition of particles for oxidative damage and carcinogenic mechanisms. J. Environ. Sci. Health Part C 26 (4), 339–362. https://doi.org/10.1080/10590500802494538.

Vianello, A., Jensen, R.L., Liu, L., Vollertsen, J., 2019. Simulating human exposure to indoor airborne microplastics using a breathing thermal manikin. Sci. Rep. 9, 8670. https://doi.org/10.1038/s41598-019-45054-w.

Waller, C.L., Griffiths, H.J., Waluda, C.M., Thorpe, S.E., Loaiza, I., Moreno, B., Pacherres, C.O., Hughes, K.A., 2017. Microplastics in the Antarctic marine system: an emerging area of research. Sci. Total Environ. 598, 220–227. https://doi.org/10.1016/j.scitotenv.2017.03.283.

Watson, C.Y., DeLoid, G.M., Pal, A., Demokritou, P., 2016. Buoyant nanoparticles: implications for nano-biointeractions in cellular studies. Small 12 (23), 3172–3180. https://doi.org/10.1002/smll.201600314.

Xu, M., Halimu, G., Zhang, Q., Song, Y., Fu, X., Li, Y., Li, Y., Zhang, H., 2019. Internalization and toxicity: a preliminary study of effects of nanoplastic particles on human lung epithelial cell. Sci. Total Environ. 694, 133794. https://doi.org/10.1016/j.scitotenv.2019.133794.

Zhang, Y., Kang, S., Allen, S., Allen, D., Gao, T., Sillanpää, M., 2020. Atmospheric microplastics: a review on current status and perspectives. Earth-Sci. Rev. 203, 103118. https://doi.org/10.1016/j.earscirev.2020.103118.

Zhao, H.-J., Xu, J.-K., Yan, Z.-H., Ren, H.-Q., Zhang, Y., 2020. Microplastics enhance the developmental toxicity of synthetic phenolic antioxidants by disturbing the thyroid function and metabolism in developing zebrafish. Environ. Int. 140, 105750. https://doi.org/10.1016/j.envint.2020.105750.

Zhu, L., An, L., Ran, D.i., Lizarraga, R., Bondy, C., Zhou, X.u., Harper, R.W., Liao, S.-Y., Chen, Y., 2019. The club cell marker SCGB1A1 downstream of FOXA2 is reduced in asthma. Am. J. Respir. Cell Mol. Biol. 60 (6), 695–704. https://doi.org/10.1165/rcmb.2018-0199OC.